Journal of Elasticity
https://doi.org/10.1007/s10659-023-10000-5

Gels: Energetics, Singularities, and Cavitation

M. Carme Calderer[1] · Duvan Henao[2] · Manuel A. Sánchez[3] · Ronald A. Siegel[4] · Sichen Song[4,1]

Dedicated to Jerry Ericksen, scientist, teacher and mentor: bringing in new expertise and the next generation of scholars

Received: 2 November 2022 / Accepted: 14 February 2023

Abstract
This article studies equilibrium singular configurations of gels and addresses open questions concerning gel energetics. We model a gel as an incompressible, immiscible and saturated mixture of a solid polymer and a solvent that sustain chemical interactions at the molecular level. We assume that the energy of the gel consists of the elastic energy of its polymer network plus the Flory-Huggins energy of mixing. The latter involves the entropic energies of the individual components plus that of interaction between polymer and solvent, with the temperature dependent Flory parameter, χ, encoding properties of the solvent. In particular, a *good solvent* promoting the mixing regime, is found below the threshold value $\chi = 0.5$, whereas the phase separating regime develops above that critical value. We show that cavities and singularities develop in the latter regime. We find two main classes of singularities: (i) drying out of the solvent, with water possibly exiting the gel domain through the boundary, leaving behind a core of exposed polymer at the centre of the gel; (ii) cavitation, in response to traction on the boundary or some form of negative pressure, with a cavity that can be either void or flooded by the solvent. The straightforward and unified mathematical approach to treat all such singularities is based on the construction of appropriate test functions, inspired by the particular states of uniform swelling or compression. The last topic of the article addresses a statistical mechanics rooted controversy in the research community, providing an experimental and analytic study in support of the phantom elastic energy versus the affine one.

Keywords Gels · Cavitation · Singularities · Nonlinear elasticity · Flory-Huggins · Logarithmic energies

Mathematics Subject Classification (2020) 35B40 · 35J57 · 74B20 · 74G65 · 74R99

1 Introduction

This article addresses singular phenomena in gels as well as modeling issues related to its mechanics. The former refers to cavitation, and its connection with phase separation, an

Extended author information available on the last page of the article

ubiquitously observed behavior in gels. The second involves an experimentally and analytically guided study of the elastic energy of gels as formulated across different scientific communities involved in the highly interdisciplinary field of gel research. We model the gel as an immiscible, incompressible and saturated mixture of polymer network and solvent, and in contact with its own fluid. A mixture is said to be incompressible if each one of the individual components has such a property. Immiscibility is concerned with the dependence of the constitutive equations on the volume fraction of each component. A mixture is saturated if no component, other than polymer and solvent is present, and so the volume fractions of the latter naturally add up to one.

Mixture theory was first introduced by Gibbs as a theory of fluid mixtures [17], and shortly after found its application in the study of alloys, as documented in the book by Penrose and Lebowitz [26]. In such a context, one or more of the fluid components was replaced by solid metals. The solid aspect of such emerging works awoke Ericksen's appeal to the theory, as reported in his monograph, *Introduction to the Thermodynamics of Solids* ([12], Chap. 8). Although he refers to his own work as an 'Elementary Theory', he establishes fundamental properties of thermodynamics of mixtures, when solids are involved, such as the scaling properties of the Helmholtz free energy F and the entropy with respect to the components. The Gibbs thermodynamic potential, $G = F + pV$, denoting V the volume of the region partially occupied by solids and p the pressure, plays a main role. He regards the fluid surrounding the region V as a *loading device which can do work on the solids.*

From a different point of view, Ericksen also had the foresight of identifying the difficulties that may arise when one of the components of the mixture vanishes from a location in the domain, pointing to issues of smoothness of the constitutive equations and balance laws. In the present article, we come across such difficulties, in our modeling of cavities and dry spots in the gel. Starting in the early 1960's, mixture theory took a center stage in the Continuum Mechanics research, with a major contribution by Truesdell, Ericksen and collaborators at the Johns Hopkins University. In particular, the theory was formulated to became amenable to analysis and partial differential equations. A sample of the rich literature that emerged from those efforts includes studies of chemically reacting mixtures of gases [10], liquid crystals [9], elasticity and diffusion, with temperature effects [3, 8], among others. These works later proved very relevant in applications to poroelasticity in geophysics and models for oil recovery.

The theory of mixtures of polymer and solvent was pioneered by Flory and Huggins within the framework of statistical mechanics, acknowledging that the resulting gel is indeed a new material, different from its individual components [13–15, 19]. The application of the mixture theory to crosslinked polymers, that brought in the elasticity contribution was carried out by Flory and Rehner [16]. The treatment of ionic effects in the solvent component of gels became prominent in the Japanese school following works by Tanaka and collaborators [11, 18, 27, 31–33]. If, in addition, electrically charged polymers are taken into account, observed swelling (and also compressing) rates may reach an order higher than 500 percent, bringing up again the importance of a sound formulation of the elastic energy of the gel, with Ericksen's skills becoming again very much relevant.

Properties of the gels can be, in part, inferred from their solvent and, in particular, we can distinguish between a good solvent and a θ-solvent. Water is the typical good solvent, with the slight charge separation of its molecules inducing an expanding effect in the polymer; this is due to the mixing effect, a consequence of the dominance of the polymer-solvent interaction. In a θ-solvent, the polymer tends to become clustered as a result of the primary polymer-polymer interaction. The temperature at which the latter interaction becomes of the same order as the steric effects is known as the θ-temperature [22].

In this paper, we address questions of the gel energetics and also explore issues of singularities forming in gels. The energy of a gel consists of the elastic contribution of the polymer network, defined in the reference configuration of its domain, plus the Flory-Huggins energy depending on the volume fractions of the components in the deformed gel domain. The latter consists of the entropic energy of the individual components plus that of interaction between polymer and solvent. The latter is encoded in the temperature dependent parameter $\chi > 0$, the Flory parameter, reflecting the solvent properties, and dictate whether component mixing or phase separation occur. In our model, the good solvent regime corresponds to $\chi < 0.5$, θ solvent to $\chi = 0.5$, $\chi > 0.5$ is the poor solvent regime. The singular behavior that we analyze takes place in the latter regime.

The great bulk of works in gel mechanics dealing with crosslinked polymers use the neo-Hookean energy to model the elastic deformation of polymers. Owing to its statistical mechanics derivation, the use of such a model in the literature differs on whether the logarithmic term of the Jacobian determinant of the deformation map is included or not, resulting in the so called *affine* or *phantom* models of polymer distortion, respectively. A full discussion of this issue, with the supporting references, is presented in Sect. 4. Our conclusion in favor of the phantom model is based on own experimental analysis together with an analytic proof, all carried out within the good solvent regime of the gel. We think that clarifying such an issue, in addition to its intellectual value, it also may provide a service to the gel community, since, it is, otherwise, very difficult to compare results from different workers that use the different energy formats.

The formation of voids in gels may happen due to causes analogous to those of polymer networks, such as some inherent weaknesses in the material or other unspecified triggers. Two types of responses have been identified and investigated. A rapid rearrangement of the polymer network near the newly formed cavity that reaches a stable state. An unstable response has also been observed in some cases leading to the development of fracture. While the latter event is irreversible, the first one is reversible, with the material having the ability to close down the cavity under proper conditions. The occurrence of either of such events has been linked to the type of solvent, with the reversible behavior being associated with a good solvent and the irreversible fracture to a θ solvent [22].

The mathematical treatments of cavitation in nonlinear elasticity as well as in gels, including ours, are built of spherically symmetric configurations of the material. Pence and coworkers studied cavitation by swelling, without accounting for the explicit presence of solvent, arriving at compelling and physically realistic results [25]. In work by Duda and coauthors, the model includes solvent and the Flory-Huggins interaction. Our independently developed approach yields results fully consistent with the former, in a simpler and straightforward fashion. Moreover, most of our parameters are obtained from our own experimental work.

The role of cavitation and formation of singularities in gels tends to be physically more complex than the analogous phenomena in liquids and in elastic solids, and to our knowledge has much less studied than the two former cases. In particular, the properties of the solvent as well as those of the interaction between solvent and polymer network add complexity to the cases that concern either only solvent or only polymer network. Indeed, this compels us to distinguish between the formation of two types of *singular structures*: (i) drying out of the solvent, with water leaving the gel domain through the boundary, leaving behind a core of polymer exposed at the centre of the gel; (ii) cavitation, in response to traction on the boundary or some form of negative pressure, with a cavity that can be either void or flooded by the solvent and, in some cases, leading to fracture.

Although not directly used in this article, we cannot ignore the decisive role of the Baker-Ericksen inequalities in the analysis of cavitation in nonlinear elasticity. In the article *Discontinous Equilibrium Solutions and Cavitation in Nonlinear Elasticity* [2], Ball shows that the Baker-Ericksen inequalities are satisfied by rank-one convex, isotropic stored energy functions, and brings up the connection, first observed by Knowles [21], between such inequalities and the monotonicity of the Cauchy stress in the radial direction. From this, it follows that the radial stress is well defined in the cavity, allowing to impose the zero radial stress (natural) boundary condition at the center. This leads to the finding that the critical load required to break the material is a multiple of the expression in the Baker-Ericksen inequalities. The same inequalities also show that, above the critical dead-load, the cavitated solution is stable (belonging to a branch of the supercritical bifurcation).

This article is organized as follows. After the first section devoted to the introduction, in Sect. 2 we present the model. Section 3 is devoted to the analysis of singular and cavitational solutions, with 3.1 devoted to voids and flooded locations and Sect. 3.2 to dry singularities. The remarks on the free energy are presented in Sect. 4, with Sect. 5 devoted to the conclusions.

2 Mechanical Model of a Gel

We assume that a gel is in contact with its own fluid and model it as a saturated, incompressible and immiscible mixture of elastic solid and fluid constituents. Let $\Omega \subset \mathbb{R}^3$ be a bounded domain, with smooth boundary, representing the reference configuration of the polymer network. The deformation of the polymer is represented by the vector field map

$$\boldsymbol{\varphi} : \mathbf{x} \in \Omega \longrightarrow \mathbf{y} \in \mathbb{R}^3. \tag{1}$$

We assume it to be continuously differentiable and will explicitly indicate possible exceptions in connection with formation of cavities. We assume that $\boldsymbol{\varphi}(\Omega)$ is either fully or partially surrounded by a fluid domain $\mathcal{R}$ that has the role of providing or taking water from the gel in processes of swelling and de-swelling, respectively. We label the polymer and fluid components with indices *1* and *2*, respectively. According to the theory of mixtures, a point $\mathbf{y}$ in the current (deformed) configuration is occupied by, both, fluid and solid at volume fractions $\phi_1 = \phi_1(\mathbf{y})$ and $\phi_2 = \phi_2(\mathbf{y})$, respectively. An immiscible mixture is such that the constitutive equations depend explicitly on the volume fractions $\phi_i, i = 1, 2$. We let ρ_i denote the mass density of the ith component (per unit volume of deformed gel). It is related to the intrinsic density, γ_i, by the equation $\rho_i = \gamma_i \phi_i$, $i = 1, 2$. Moreover $\gamma_i =$ constant, $i = 1, 2$ define a mixture with incompressible constituents, dubbed an incompressible mixture. The assumption of saturation of the mixture expressing that no species other than fluid and polymer are present, is expressed by the constraint

$$\phi_1 + \phi_2 = 1. \tag{2}$$

As a consequence, it suffices to know the volume fraction of polymer, which henceforth will be denoted simply by ϕ:

$$\phi(\mathbf{y}) := \phi_2(\mathbf{y}) = \text{(swollen) polymer vol. fraction at } \mathbf{y}. \tag{3}$$

In addition to the polymer domain Ω, the reference configuration of the gel is also characterized by the scalar field $0 \leq \phi_0(\mathbf{x}) \leq 1$, $\mathbf{x} \in \Omega$ that represents the reference volume fraction

of the polymer. The equation of balance of mass of the polymer states that, for every subset $E \subset \Omega$,

$$\int_{\boldsymbol{\varphi}(E)} \phi(\mathbf{y})\, d\mathbf{y} = \int_E \phi_0(\mathbf{x})\, d\mathbf{x}. \tag{4}$$

Formally, in the absence of cavities, it reduces to a pointwise relation

$$\phi(\boldsymbol{\varphi}(\mathbf{x}))\det F(\mathbf{x}) = \phi_0(\mathbf{x}), \quad F(\mathbf{x}) = \nabla\varphi(\mathbf{x}), \quad \text{for all} \quad \mathbf{x} \in \Omega. \tag{5}$$

We appeal to our article [30] for the detailed justification of the energy of the gel and present here a necessary summary. The total energy consists of two terms, the elastic energy of the polymer network plus the Flory-Huggins contribution of mixing the solvent and the polymer components:

$$\mathcal{E} = \int_\Omega W_{\text{el}}(\nabla\varphi(\mathbf{x}))\, d\mathbf{x} + \int_{\varphi(\Omega)} W_{\text{FH}}(\phi(\mathbf{y}))\, d\mathbf{y}. \tag{6}$$

As customary in the gel literature, we assume that W_{el} is Neo-Hookean:

$$W_{\text{el}}(\mathsf{F}) := \frac{G}{2}|\mathsf{F}|^2, \quad G > 0, \tag{7}$$

with an elastic modulus G that has dimensions of energy density. The Flory-Huggins energy density of mixing ([7, Eq. 2.62], [28, p. 143]), has the form

$$W_{\text{FH}}(\phi) := \frac{k_B T}{V_m}(\phi_1 \ln\phi_1 + \frac{1}{N}\phi_2 \ln\phi_2 + \chi\phi_1\phi_2), \quad \phi_1 := 1 - \phi, \quad \phi_2 = \phi. \tag{8}$$

Here V_m represents the volume occupied by one monomer of solvent; k_B the Boltzmann constant; $N \gg 1$ is the number of segments occupied by the polymer in the lattice model for polymer solutions (the solvent molecules being assumed to occupy each a single lattice site); and χ is the Flory-Huggins interaction parameter. The first and second terms in (8) correspond to the entropy of the polymer and fluid, respectively, and the third term represents attractive or repulsive forces between the two components.

The mixing energy density must be integrated on the current (swollen) configuration, where the interaction between the two species takes place. In order to combine it with the elastic energy, we carry out a change to the reference (Lagrangian) variables, that in the case that the deformation is regular gives

$$\int_\Omega W_{\text{FH}}\Big(\phi\big(\boldsymbol{\varphi}(\mathbf{x})\big)\Big)\, \det\mathsf{F}(\mathbf{x})\, d\mathbf{x}. \tag{9}$$

Let us introduce the notation

$$\nu := \frac{k_B T}{V_m}, \quad \gamma := \frac{G}{\nu}, \quad J := \det\mathsf{F},$$

and the dimensionless expression

$$H(J) := \frac{1}{\nu} J\, W_{\text{FH}}(\phi), \quad \phi = \phi_0/J,$$

$$= \frac{1}{N}\phi_0 \ln\frac{\phi_0}{J} + (J-\phi_0)\ln(1-\frac{\phi_0}{J}) + \phi_0\chi(1-\frac{\phi_0}{J}), \quad J > \phi_0. \tag{10}$$

We will take ν as a reference –entropic– energy density unit. Dividing the total energy of the gel by ν and by its volume in the initial state, and taking the mass balance equation (5) into account, we arrive finally at the following dimensionless quantity:

$$E = \int_\Omega \frac{\gamma}{2}|\mathsf{F}|^2 + H(J)\,dx. \tag{11}$$

Determining the values of χ such that $H(J)$ is convex and finding the critical value χ_c above which the convexity is lost is relevant to our problem [7, Sect. 2.4]. In the later case, the gel separates into the polymer and fluid phases, which is relevant to cavities forming in the gel. A direct calculation gives

$$\omega(J) := H'(J) = -\frac{1}{\nu}\Pi(\phi) = -\frac{\phi}{N} + \ln(1-\phi) + \phi + \chi\phi^2, \quad \phi = \phi_0/J, \tag{12}$$

where

$$\Pi(\phi) := -W_{\mathrm{FH}}(\phi) + \phi\frac{\mathrm{d}W_{\mathrm{FH}}}{\mathrm{d}\phi} + W_{\mathrm{FH}}(0) \tag{13}$$

is the osmotic pressure of the polymer solution. Also,

$$H''(J) = \frac{\phi}{\nu J}\frac{\mathrm{d}\Pi}{\mathrm{d}\phi} = \frac{\phi}{J}\left(\frac{1}{N} + \frac{1}{1-\phi} - 1 - 2\chi\phi\right). \tag{14}$$

Hence $H(J)$ is convex in the whole range $J \in (\phi_0, \infty)$ if and only if [7, Eq. 2.67]

$$\chi < \underbrace{\frac{1}{2}\left(1+\frac{1}{\sqrt{N}}\right)^2}_{:=\chi_c}. \tag{15}$$

This range for χ corresponds to the mixing regime for the gel [28]. Furthermore, since H is convex then the energy density $\frac{\gamma}{2}|\mathsf{F}|^2 + H(\det\mathsf{F})$ in (11) is a polyconvex function [1, 6] of the deformation gradient. The available existence theory for polyconvex energy densities (e.g., [1, 6, 24]) do not cover the low coercivity situation at hand. However, as is the case for neo-Hookean materials, under appropriate boundary conditions energy minimizers are expected to exist.

In the regime $\chi < \chi_c$ the osmotic pressure is positive. The loss of convexity of $H(J)$, corresponding to $\chi > \chi_c$ and allowing for negative osmotic pressure, is associated with cavities forming in the gel. The well-posedness of the minimization problem requires adding a regularizing term $|\nabla\phi|^2$ in the energy (6) [5, 36].

From now on, we will consider the $N \to \infty$ approximation for the mixing energy of the gel, so that $\chi_c = \frac{1}{2}$.

3 Cavitation

Throughout this section, we consider spherically symmetric configurations of the gel and assume that it occupies a spherical domain of radius $R_0 > 0$. The reference configuration of

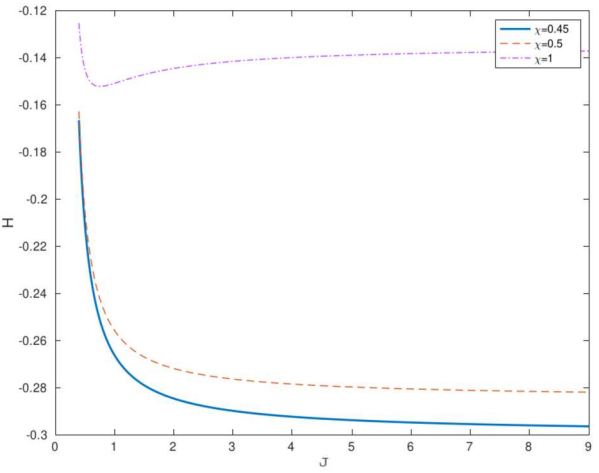

Fig. 1 Plots of $H(J)$ Note the loss of convexity of H as χ increases. The reference volume fraction is set to $\phi_0 = 0.2$ [30]

the polymer component is the domain

$$\Omega_0 = \{\mathbf{x} \in \mathbb{R}^3 : \|\mathbf{x}\| < R_1\}, \quad \phi = \phi_0 \tag{16}$$

where ϕ_0 is the volume fraction of the polymer. We study radially symmetric deformations of the gel:

$$r = r(R), \quad \theta = \Theta, \quad \varphi = \Phi, \tag{17}$$

$$\phi = \phi(R). \tag{18}$$

The deformation gradient tensor is

$$\mathsf{F} = \mathrm{diag}[r'(R), \frac{r(R)}{R}, \frac{r(R)}{R}], \quad J := \det \mathsf{F} = r'(R)\frac{r^2(R)}{R^2}. \tag{19}$$

3.1 Voids and Flooded Locations

Let us assume that some additional negative pressure appears, such as water evaporation. In order to simplify the analysis, let us represent this situation with an expansive Dirichlet condition. More precisely, we perturb the free swelling solution

$$r(R) \equiv \lambda^* R, \quad 0 \leq R < R_1, \tag{20}$$

where λ^* is obtained from the equation for the equilibrium between the elastic and the osmotic forces [30]

$$\lambda H'(\lambda^3) = -\gamma, \tag{21}$$

by imposing a further expansion of the gel through the displacement boundary condition

$$r(R_1) = \lambda R_1 \tag{22}$$

for values of $\lambda > \lambda^*$. We compare two alternative ways in which the gel can respond to this requirement. One is by means of the uniform expansion

$$r(R) \equiv \lambda R, \quad 0 \le R < R_1. \tag{23}$$

The other is by opening up a cavity, while at the same time keeping the polymer and solvent volume fractions of the swelling equilibrium state. This second alternative is obtained from the following equation:

$$J \equiv (\lambda^*)^3 \quad \Rightarrow \quad \frac{r^2 r'}{R^2} = (\lambda^*)^3 \quad \text{for all } R \tag{24}$$

$$\Rightarrow \quad (r^3)' = ((\lambda^* R)^3)' \tag{25}$$

$$\Rightarrow \quad r^3(R) = (\lambda^* R)^3 + C. \tag{26}$$

The constant C can be obtained from the boundary condition:

$$(\lambda R_1)^3 = (\lambda^* R_1)^3 + C \quad \Rightarrow \quad C = R_1^3(\lambda^3 - (\lambda^*)^3), \tag{27}$$

giving the deformation

$$r(R) = \Big((\lambda^* R)^3 + R_1^3(\lambda^3 - (\lambda^*)^3)\Big)^{1/3}. \tag{28}$$

This deformation opens up a cavity of radius:

$$\text{cavity radius} = \lim_{R \to 0^+} r(R) = R_1 \sqrt[3]{\lambda^3 - (\lambda^*)^3}, \tag{29}$$

which begins as a zero radius when $\lambda = \lambda^*$ and grows as the radial stretch λ imposed at the outer boundary becomes larger. Note that

$$\phi(r) = \begin{cases} 0 & \text{if } 0 \le r < R_1 \sqrt[3]{\lambda^3 - (\lambda^*)^3}, \\ \phi^* & \text{if } R_1 \sqrt[3]{\lambda^3 - (\lambda^*)^3} < r \le \lambda R_1, \end{cases} \qquad \phi^* = \frac{\phi_0}{(\lambda^*)^3},$$

where ϕ^* is the polymer volume fraction at swelling equilibrium. (We point out that, both, the radial distance r and the current polymer volume fraction ϕ are defined in the deformed configuration).

The energy of the uniform expansion, compared to the energy at swelling equilibrium, is

$$E_1(\lambda) = \Big(\frac{4\pi}{3} R_1^3\Big) \cdot \Big(\frac{G}{2} \cdot 3(\lambda^2 - (\lambda^*)^2) + \frac{k_B T}{V_m}\big(H(\lambda^3) - H((\lambda^*)^3)\big).\Big) \tag{30}$$

The energy of the cavitated configuration, also compared to the energy of the swelling equilibrium, is

$$E_2(\lambda) = \int_0^{R_1} (4\pi R^2 dR) \cdot \Big(\frac{G}{2}\big(r'(R)^2 + 2\frac{r^2(R)}{R^2} - 3(\lambda^*)^2\big) \tag{31}$$

$$+ \frac{k_B T}{V_m}\Big(H\big(r'(R)\frac{r^2}{R^2}\big) - H\big((\lambda^*)^3\big)\Big)\Big) \tag{32}$$

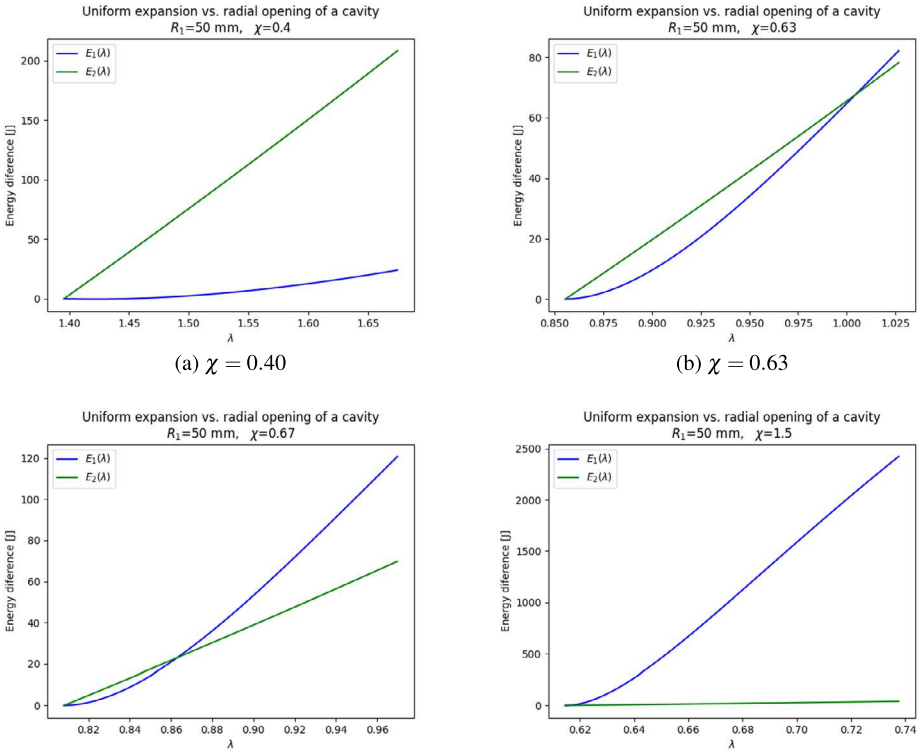

(a) $\chi = 0.40$ (b) $\chi = 0.63$

(c) $\chi = 0.67$ (d) $\chi = 1.50$

Fig. 2 Comparison of the energies of a uniformly expanded state (blue) and that of a configuration with a void (green), for different values of χ

$$= 4\pi \int_0^{R_1} R^2 \cdot \frac{G}{2}\left(\left(\frac{(\lambda^*)^3 R^2}{r(R)^2}\right)^2 + 2\frac{r(R)^2}{R^2}\right) dR - \frac{4\pi}{3} R_1^3 \cdot \frac{G}{2} \cdot 3(\lambda^*)^2, \tag{33}$$

since, in this case, the Jacobian is constant and equal to $(\lambda^*)^3$. The above relation can also be written as

$$\frac{E_2(\lambda)}{4\pi} = \int_0^{R_1} R^2 \hat{W}(v(R)) dR - \frac{R_1^3}{3} \hat{W}(\lambda^*),$$

with

$$\hat{W}(v) := \frac{G}{2}((\lambda^*)^6 v^{-4} + 2v^2), \quad v(R) := \frac{r(R)}{R}. \tag{34}$$

Following [2, Eq. (5.27)], we observe that

$$v(R)^3 = R^{-3}\Big((\lambda^* R)^3 + R_1^3(\lambda^3 - (\lambda^*)^3)\Big) = (\lambda^*)^3 + R_1^3(\lambda^3 - (\lambda^*)^3)R^{-3}$$

$$R^3 = \frac{R_1^3(\lambda^3 - (\lambda^*)^3)}{v^3 - (\lambda^*)^3}, \quad \frac{d}{dR}\Big(\hat{W}\big(v(R)\big)\Big) = \frac{d\hat{W}}{dv}\frac{dv}{dR}.$$

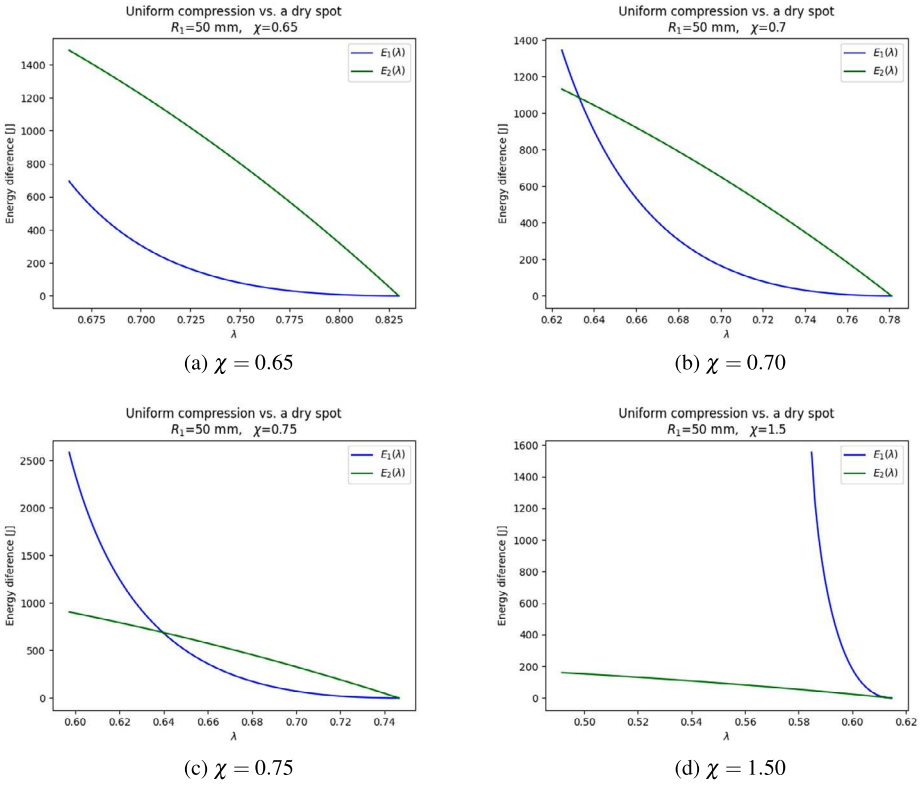

(a) $\chi = 0.65$ (b) $\chi = 0.70$

(c) $\chi = 0.75$ (d) $\chi = 1.50$

Fig. 3 Comparison of the energies of a uniformly compressed state (blue) and that of a configuration with a dry spot (green), for different values of χ

Integrating by parts yields

$$\frac{E_2(\lambda)}{4\pi} = \frac{R_1^3(\lambda^3 - (\lambda^*)^3)}{3(v^3 - (\lambda^*)^3)} \hat{W}\big(v(R)\big)\Big|_{R=0}^{R_1} - \frac{1}{3}\int_0^{R_1} \frac{R_1^3(\lambda^3 - (\lambda^*)^3)}{v^3 - (\lambda^*)^3} \frac{d\hat{W}}{dv}\frac{dv}{dR} dR - \frac{R_1^3}{3}\hat{W}(\lambda^*).$$

Note that, as $R \to 0^+$, the tangential stretch $v(R) = \frac{r(R)}{R}$ tends to infinity due to the opening of the cavity. Hence,

$$\frac{E_2(\lambda)}{\frac{4\pi}{3}R_1^3} = \hat{W}(\lambda) - \hat{W}(\lambda^*) + (\lambda^3 - (\lambda^*)^3)\int_\lambda^\infty \frac{1}{v^3 - (\lambda^*)^3}\frac{d\hat{W}}{dv} dv.$$

Now,

$$\frac{d\hat{W}}{dv} = 2G(v - (\lambda^*)^6 v^{-5}) = 2Gv^{-5}(v^6 - (\lambda^*)^6) = 2Gv^{-5}(v^3 + (\lambda^*)^3)(v^3 - (\lambda^*)^3).$$

Therefore,

$$\begin{aligned}\frac{E_2(\lambda)}{\frac{4\pi}{3}R_1^3} &= \hat{W}(\lambda) - \hat{W}(\lambda^*) + 2G(\lambda^3 - (\lambda^*)^3)\int_\lambda^\infty v^{-5}(v^3 + (\lambda^*)^3)dv \\ &= \hat{W}(\lambda) - \hat{W}(\lambda^*) + 2G(\lambda^3 - (\lambda^*)^3)\int_\lambda^\infty v^{-2} + (\lambda^*)^3 v^{-5}dv \\ &= \hat{W}(\lambda) - \hat{W}(\lambda^*) + \frac{G}{2}(\lambda^3 - (\lambda^*)^3)\Big(4\lambda^{-1} + (\lambda^*)^3\lambda^{-4}\Big).\end{aligned}$$

Figure 2 show the energetically prevalent configuration for different values of the Flory parameter χ. For a related stability analysis, we calculate the derivatives of both expressions with respect to λ, evaluated at $\lambda = \lambda^*$:

$$\frac{\frac{dE_1}{d\lambda}}{\frac{4\pi}{3}R_1^3} = 3G\lambda + \frac{k_BT}{V_m}H'(\lambda^3)\cdot 3\lambda^2 = \frac{3K_BT}{V_m}(\gamma\lambda + \lambda^2 H'(\lambda^3)).$$

Evaluating it $\lambda = \lambda^*$ and using equation (21) also at λ^*, we find that

$$\frac{\mathrm{d}E_1}{\mathrm{d}\lambda}\bigg|_{\lambda=\lambda^*} = 0.$$

The second derivative is given by

$$\frac{\frac{d^2E_1}{d\lambda^2}}{\frac{4\pi}{3}R_1^3} = \frac{3K_BT}{V_m}(\gamma + 2\lambda H'(\lambda^3) + 3\lambda^4 H''(\lambda^3)).$$

At $\lambda = \lambda^*$, we obtain

$$\frac{d^2E_1}{d\lambda^2}\bigg|_{\lambda=\lambda^*} = 4\pi R_1^3\frac{K_BT}{V_m}(-\gamma + 3(\lambda^*)^4 H''((\lambda^*)^3)).$$

Let us now carry out the analogous calculations for E_2,

$$\frac{\frac{dE_2(\lambda)}{d\lambda}}{\frac{4\pi}{3}R_1^3} = \frac{3G}{2}(4\lambda + (\lambda^*)^3\lambda^{-2}), \quad \text{and}$$

$$\frac{\frac{d^2E_2(\lambda)}{d\lambda}}{\frac{4\pi}{3}R_1^3} = \frac{3G}{2}(4 - 2(\lambda^*)^3\lambda^{-3}).$$

Gathering the expressions for E_1 and E_2 we find that

$$\frac{d}{d\lambda}(E_2(\lambda) - E_1(\lambda))\bigg|_{\lambda=\lambda^*} = 10\pi R_1^3 G\lambda^* > 0,$$

$$\frac{d^2}{d\lambda^2}(E_2(\lambda) - E_1(\lambda))\bigg|_{\lambda=\lambda^*} = 4\pi R_1^3\frac{k_BT}{V_m}(2\gamma - 3(\lambda^*)^4 H''((\lambda^*)^3)).$$

In conclusion, we find that when λ starts growing above λ^*, the cavitation solution becomes energetically higher than the homogeneous deformation. However, for values of $\chi > \frac{1}{2}$ (that

is, in the phase-separation regimen when $H(J)$ is not convex), after a small energetic barrier is overcome, the cavitation solution has less energy than the homogeneous expansion.

3.2 Dry Spots

We now consider a similar analysis, but with $\lambda < \lambda^*$. We compare the homogeneous deformation $r(R) \equiv \lambda R$ against the following second alternative:

$$r(R) := \begin{cases} \phi_0^{1/3} R & \text{if } R \le R_\lambda \\ \Big((\lambda^* R)^3 + R_1^3 (\lambda^3 - (\lambda^*)^3) \Big)^{1/3} & \text{if } R_\lambda \le R \le R_1. \end{cases} \tag{35}$$

This solution is characterized by the fact that

$$\phi\big(r(R)\big) = \begin{cases} 1 & R < R_\lambda \\ \phi^* & R_\lambda < R < 1, \end{cases} \qquad \phi^* = \frac{\phi_0}{(\lambda^*)^3}. \tag{36}$$

The fluid is taken away from the subregion $B(0, R_\lambda)$ in the centre of the reference configuration, leaving the polymer exposed.

The value of R_λ is determined by the requirement of continuity of the deformation map at $R = R_\lambda$:

$$\phi_0 R_\lambda^3 = (\lambda^* R_\lambda)^3 + R_1^3 (\lambda^3 - (\lambda^*)^3), \tag{37}$$

giving

$$R_\lambda^3 = \frac{(\lambda^*)^3 - \lambda^3}{(\lambda^*)^3 - \phi_0} R_1^3. \tag{38}$$

We assume that $\lambda^3 > \phi_0$ so that the radius R_λ, thus defined, is less than R_1.

When $\chi < \frac{1}{2}$, the energy density is polyconvex and it can be shown that the homogeneous deformation (the first alternative) is the global minimizer (even compared to non-radially symmetric deformations). Indeed, the deformation given by $r(R)$ above is in $W^{1,\infty}$, and polyconvexity, as is well known [1], implies $W^{1,\infty}$-quasiconvexity. More specifically, for the affine Dirichlet boundary data $\varphi(\mathbf{x}) = \lambda \mathbf{x}$ for $\mathbf{x} \in \Omega_0$, Jensen's inequality yields:

$$\fint_{\Omega_0} \frac{G}{2} |\nabla \varphi|^2 + H(\det \nabla \varphi)\, d\mathbf{x} \ge \frac{G}{2} \left| \fint_{\Omega_0} \nabla \varphi \, d\mathbf{x} \right|^2 + H\left(\int_{\Omega_0} \det \nabla \varphi \, d\mathbf{x} \right).$$

For all $\varphi \in W^{1,3}(\Omega_0, \mathbb{R}^3)$ that are one-to-one a.e. and satisfy $\det \nabla \varphi > 0$ a.e. and the boundary condition, both integrals on the right-hand side coincide with the corresponding expressions for the affine deformation $\mathbf{x} \mapsto \lambda \mathbf{x}$. Hence, the dry spot will not be seen. However, in the phase-separation regime, when $\chi > \frac{1}{2}$ and $H(J)$ is not convex in J, the second alternative might have a better energy.

The energy of the homogeneous deformation, compared against the energy at swelling equilibrium, is given by equation (30). The energy of the competing dry cavity (35) is

$$\frac{E_2(\lambda)}{\frac{4\pi}{3} R_1^3} = R_1^{-3} \int_{R_\lambda}^{R_1} (3R^2 dR) \Big(\hat{W}(v(R)) + \frac{k_B T}{V_m} H\big(r'(R) v(R)^2\big) \Big)$$

$$
\begin{aligned}
&+\frac{R_\lambda^3}{R_1^3}\Big(\frac{3G}{2}\phi_0^{2/3}+\frac{k_BT}{V_m}\lim_{J\to\phi_0^-}H(J)\Big)-\frac{G}{2}\cdot 3(\lambda^*)^2-\frac{k_BT}{V_m}H((\lambda^*)^3)\\
&=R_1^{-3}R^3\hat{W}(v(R))\Big|_{R=R_\lambda}^{R_1}-R_1^{-3}\int_{R_\lambda}^{R_1}\frac{R_1^3((\lambda^*)^3-\lambda^3)}{(\lambda^*)^3-v^3}\frac{d\hat{W}}{dv}\frac{dv}{dR}dR\\
&-R_1^{-3}\frac{k_BT}{V_m}H((\lambda^*)^3)R_\lambda^3+\frac{R_\lambda^3}{R_1^3}\cdot\frac{3G}{2}\phi_0^{2/3}-\hat{W}(\lambda^*)\\
&=\hat{W}(\lambda)-\hat{W}(\lambda^*)-\frac{R_\lambda^3}{R_1^3}\hat{W}(\phi_0^{1/3})-((\lambda^*)^3-\lambda^3)\int_{\phi_0^{1/3}}^{\lambda}\frac{1}{(\lambda^*)^3-v^3}\frac{d\hat{W}}{dv}dv\\
&+\frac{R_\lambda^3}{R_1^3}\Big(\frac{3G}{2}\phi_0^{2/3}-\frac{k_BT}{V_m}H((\lambda^*)^3)\Big)\\
&=\hat{W}(\lambda)-\hat{W}(\lambda^*)+((\lambda^*)^3-\lambda^3)\frac{\frac{G}{2}\phi_0^{-4/3}(\phi_0^2-(\lambda^*)^6)-\frac{k_BT}{V_m}H((\lambda^*)^3)}{(\lambda^*)^3-\phi_0}\\
&+((\lambda^*)^3-\lambda^3)\int_{\phi_0^{1/3}}^{\lambda}2G(v^{-2}+(\lambda^*)^3v^{-5})dv
\end{aligned}
$$

Using again the expression (34), we find

$$
\begin{aligned}
\frac{E_2(\lambda)}{\frac{4\pi}{3}R_1^3}&=\hat{W}(\lambda)-\hat{W}(\lambda^*)+((\lambda^*)^3-\lambda^3)\frac{\frac{G}{2}\phi_0^{-4/3}(\phi_0^2-(\lambda^*)^6)-\frac{k_BT}{V_m}H((\lambda^*)^3)}{(\lambda^*)^3-\phi_0}\\
&+((\lambda^*)^3-\lambda^3)\frac{G}{2}(4\phi_0^{-1/3}+(\lambda^*)^3\phi_0^{-4/3}-4\lambda^{-1}-(\lambda^*)^3\lambda^{-4})\\
&=\hat{W}(\lambda)-\hat{W}(\lambda^*)\\
&+((\lambda^*)^3-\lambda^3)\Bigg(\frac{G}{2}\Big(4\phi_0^{-1/3}+(\lambda^*)^3\phi_0^{-4/3}-4\lambda^{-1}-(\lambda^*)^3\lambda^{-4}\Big)\\
&-\frac{G}{2}\Big((\lambda^*)^3\phi_0^{-4/3}+\phi_0^{-1/3}\Big)-\frac{k_BT}{V_m}\frac{H((\lambda^*)^3)}{(\lambda^*)^3-\phi_0}\Bigg)\\
&=\hat{W}(\lambda)-\hat{W}(\lambda^*)\\
&+((\lambda^*)^3-\lambda^3)\Big(\frac{G}{2}\Big(3\phi_0^{-1/3}-4\lambda^{-1}-(\lambda^*)^3\lambda^{-4}\Big)-\frac{k_BT}{V_m}H((\lambda^*)^3)\Big).
\end{aligned}
$$

Figure 3 shows the energy of the uniformly compressed and cavitated state for different values of the Flory parameter χ. In conclusion,

$$
\begin{aligned}
\frac{E_2(\lambda)}{\frac{4\pi}{3}R_1^3}=&((\lambda^*)^3-\lambda^3)\Big(\frac{3G}{2}(\phi_0^{-1/3}-\lambda^{-1})-\frac{k_BT}{V_m}H((\lambda^*)^3)\Big)\\
&-\frac{3G}{2}((\lambda^*)^2-\lambda^2).
\end{aligned}
\tag{39}
$$

Now, we compute the derivative with respect to λ. For the homogeneous deformation the expressions are the same as in the case when $\lambda>\lambda^*$. Regarding the deformation creating a

dry spot, we have

$$\frac{\frac{dE_2(\lambda)}{d\lambda}}{\frac{4\pi}{3}R_1^3} = \frac{3G}{2}((\lambda^*)^3\phi_0^{-1/3} + 4\lambda) + 3\frac{k_BT}{V_m}H((\lambda^*)^3)\lambda^2. \tag{40}$$

Evaluating it at $\lambda = \lambda^*$, we find:

$$\frac{d}{d\lambda}(E_2(\lambda) - E_1(\lambda))\bigg|_{\lambda=\lambda^*} = 4\pi R_1^3\Big(\frac{G}{2}\big((\phi_0^{-1/3} + 4)\lambda^* - 3\phi_0^{-1/3}(\lambda^*)^2\big) + \frac{k_BT}{V_m}H((\lambda^*)^3)(\lambda^*)^2\Big). \tag{41}$$

4 Remarks on the Elastic Energy Density

By means of the experimental and analytic studies presented next, we justify the validity of the phantom energy model of the gel, that is, neglecting the logarithmic term in the elastic energy of the polymer, versus the competitor affine model. For this, we continue experimental results reported in [30] on the swelling of a thin rectangular polyacrylamide (PAAm) gel completely bonded to a rigid substrate. Specifically, we report that the phantom model for the elastic distortion gives a better agreement, compared to the affine model, with our lateral swelling experiments. We conclude the section with an analytic proof, which is valid in the mixture regime.

In the statistical mechanics derivation of the Gaussian model for polymers different expressions are obtained for the elastic distortion energy density according to whether the gel is assumed to follow the same affine deformation as the infinitesimal polymer block that is subject to a homogeneous deformation. When that assumption is made, the resulting expression, which includes a logarithmic term:

$$W_{\text{aff}}(\mathsf{F}) = \frac{G}{2}(|\mathsf{F}|^2 - 3) - G\ln J, \tag{42}$$

is known as the affine model for the elastic distortion (see, e.g., [13, 20, 23, 34, 35]). In contrast, in the phantom model for the elastic distortion, where the polymer chains are allowed to move freely through one another and the network junctions fluctuate around their mean positions, the resulting expression is just

$$W_{\text{ph}}(\mathsf{F}) = \frac{G}{2}(|\mathsf{F}|^2 - 3) \tag{43}$$

(see, e.g., [7, Sects. 3.3.1, 3.3.2, 3.4.1], [23, 34]). For a solid incompressible polymer, the expressions are equivalent. However, when the polymers are exposed to a solvent and an accurate description of the volume increase due to solvent absorption, it is unclear whether the affine or the phantom model should be considered. In this section we report results based on finite element simulations comparing both models against experimental results of the lateral swelling in a thin PAAm gel fully bonded to a glass substrate. A better agreement is found with the phantom model.

The finite element simulations for the affine and phantom model are compared against our experimental work reported in [30] (Sect. 2). Numerical simulations are implemented (as those in [30] (Sect. 4.1) in the open-source finite element library Netgen/NGSolve (www.

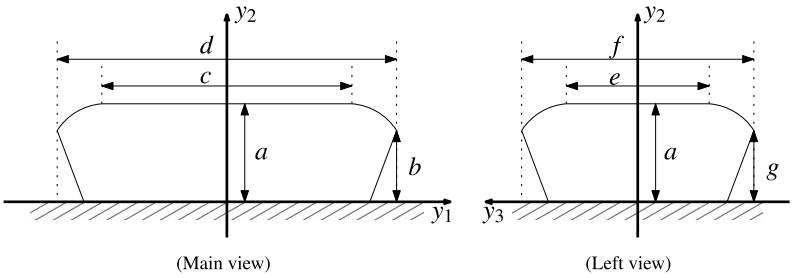

Fig. 4 Shapes of a completely bonded gel at swelling equilibrium. The illustration exaggerates the rounding-off at the upper corners, and the outward displacement of the lateral surfaces (the actual aspect ratio d/a, in the main view, is of the order of 94 : 3, as can be seen in Table 1. The frame y_1, y_2, y_3, with the notation used in the expressions $\mathbf{y} = \mathbf{x} + \mathbf{u}(\mathbf{x})$, $\mathbf{x} = (x_1, x_2, x_3)$, $\mathbf{y} = (y_1, y_2, y_3)$ in the mathematical model, is depicted with heavy lines (in particular, the vertical direction is denoted by y_2) [30]

Table 1 Experimental and finite element simulation results for the swelling of a 90.0 [mm] × 1.62 [mm] × 15.0 [mm] rectangular PAAm gel completely bonded to a glass slide, data from [30]

Configuration	a	b	c	d	e	f	g
Reference	1.62	1.62	90.0	90.0	15.0	15.0	1.62
Gel 1	3.31	2.05	88.08	93.90	11.42	19.00	1.75
Gel 2	3.35	2.13	88.39	93.85	11.68	18.99	1.78
Gel 3	3.50	2.01	88.31	93.56	11.49	18.79	1.72
Gel 4	3.45	2.23	88.25	93.62	11.86	19.00	1.64
Average	3.40	2.11	88.26	93.73	11.61	18.95	1.72
SD	0.09	0.10	0.13	0.17	0.20	0.10	0.06
Affine model	3.02	1.76	87.64	93.70	12.62	18.80	1.70
Phantom model	3.19	1.72	86.96	93.98	12.27	19.12	1.65

ngsolve.org) [29]. The computational domain is discretized with tetrahedral meshes and continuous piecewise cubic finite element spaces are used to approximate the displacement variable. The resulting system of nonlinear boundary value problems are solved with a damped Newton's method. In order to have an adequate initial condition for Newton's scheme, the 'incremental softening' technique is applied, consisting in solving first the nonlinear system for more rigid gels (with shear moduli of five or ten times larger than the measured $G = 0.13$ MPa).

4.1 Measurements

Table 1 presents the experimental and the finite elements results for both the affine and the phantom model. The gel is observed to swell mostly in the direction normal to the substrate, since the attempt to swell along the width and length directions is largely prevented by the constraining glass slide. Nevertheless, as one moves away from the substrate, a small and increasing amount of lateral swelling can indeed be observed. In order to quantitatively describe this 'bread loafing' effect, measurements a, b, c, d, e, f, and g are made as depicted in Fig. 4.

As can be seen in Table 1, the amount of lateral displacement is observed to be very similar in the two horizontal directions, close to 2 mm on each side: the difference of 3.73 mm between the measurement d and the length of 90.0 mm of the gel in its initial state, accounts

for the sum of the displacements towards the left and towards the right of the sample. The difference of 3.95 mm between the measurement f and the initial width of 15.0 mm accounts for the displacement towards the back and the front. The largest deformation occurs in the direction normal to the substrate, where the gel reaches a thickness of 3.40 mm (measurement a made in the middle of the sample). Given the initial thickness of 1.62 mm, this corresponds to a vertical extension of:

$$\lambda = \frac{3.40}{1.62} = 2.0988, \tag{44}$$

that is, it stretches by approximately 110%.

Regarding the numerical simulations, as explained in [30] they are obtained by minimizing the energy functional

$$\int_\Omega W_{\rm el}(\mathsf{F}) + \frac{k_B T}{V_m}\Big((J-\phi_0)\ln(1-\phi) + \chi\phi_0(1-\phi)\Big)\,\mathrm{d}\mathbf{x}, \quad J = \det\mathsf{F}, \quad \phi = \frac{\phi_0}{J},$$

where $\mathsf{F} = \mathsf{I} + \nabla\mathbf{u}$ is the deformation gradient. As explained in [30] (Sect. 4 and Appendix), the penalty term $10^5 \cdot \int |(x_2 + u_2(\mathbf{x}))^-|^2\,\mathrm{d}\mathbf{x}$ is also added in order to prevent an unphysical interpenetration of the glass substrate due to a protrusion originated from the left and right facets. The polymer volume fraction ϕ_0 in the reference configuration is approximately $\phi = 0.20$ (see [30] (Sect. 2.2.1) for more details on the synthesis of the PAAm gel). In the simulations the values for k_B and V_m were $1.38\cdot 10^{-23}$ m^2 kg s^{-2} K^{-1} and $3\cdot 10^{-29}$ m^3, yielding an approximate value of 136.6 MPa for the prefactor $\frac{k_B T}{V_m}$ in the Flory-Huggins term.

The value of the Flory parameter χ was obtained from our free swelling experiments reported in [30] (Sect. 2.3.1), the results of which are summarized in Table 2. The resulting value of χ depends on whether the affine or the phantom model is adopted for the elastic distortion. In the three repetitions of the experiment a homogeneous deformation was observed, very close to an isotropic expansion, as predicted by the model. The volume at swelling equilibrium was approximately $J_{\rm iso} = 3.29$ times the volume of the reference configuration. The pointwise energy minimizers of the above energy density are of the form $\mathsf{F} = \lambda\mathsf{R}$, where R is a rotation and λ is obtained from the condition of equilibrium of forces:

$$\mathsf{P}(\lambda\mathsf{I}) = 0, \quad \mathsf{P}(\mathsf{F}) = \frac{\partial W_{\rm el}(\mathsf{F})}{\partial \mathsf{F}} + \frac{k_B T}{V_m} H'(J)\mathsf{F}^c, \tag{45}$$

where P is the Piola-Kirchhoff stress tensor and where by F^c we have denoted the cofactor matrix of F. For the phantom model this gives [30] (Sect. 3.4)

$$\chi_{\rm ph} = -(\phi^\star)^{-2}\Big(\gamma J_{\rm iso}^{-1/3} + \ln(1-\phi^\star) + \phi^\star\Big), \quad \phi^\star = \frac{\phi_0}{J_{\rm iso}}, \quad \gamma = \frac{G}{k_B T/V_m} \tag{46}$$

whereas for the affine model

$$\chi_{\rm aff} = -(\phi^\star)^{-2}\Big(\gamma J_{\rm iso}^{-1/3} - \gamma J_{\rm iso}^{-1} + \ln(1-\phi^\star) + \phi^\star\Big), \quad \phi^\star = \frac{\phi_0}{J_{\rm iso}}. \tag{47}$$

The PAAm gel samples prepared were found [30] (Sect. 2.3.3) to have an elastic modulus of $G = 0.13$ MPa, thus yielding

$$\chi_{\rm ph} = 0.348, \quad \chi_{\rm aff} = 0.426. \tag{48}$$

Table 2 Shape of PAAm gels at swelling equilibrium with reference configuration of 90.0 mm × 3.0 mm × 23.5 mm ($n = 3$). The average Jacobian determinant in equilibrium is 3.2908 (standard deviation 0.0068), which corresponds to a ratio of isotropic extension $\hat{\lambda}_{\text{iso}} := J^{1/3} = 1.4874$, from [30]

Configuration	Length (mm)	Width (mm)	Thickness (mm)	Jacobian determinant J
Reference	90.0	23.5	3.0	1
Gel 1	134.24	34.69	4.48	3.2880
Gel 2	134.49	34.68	4.47	3.2858
Gel 3	134.62	34.78	4.47	3.2908
Average	134.45	4.47	34.72	3.2908
SD	0.19	0.0058	0.055	0.0068
Strecth factor	1.4865	1.4911	1.4773	

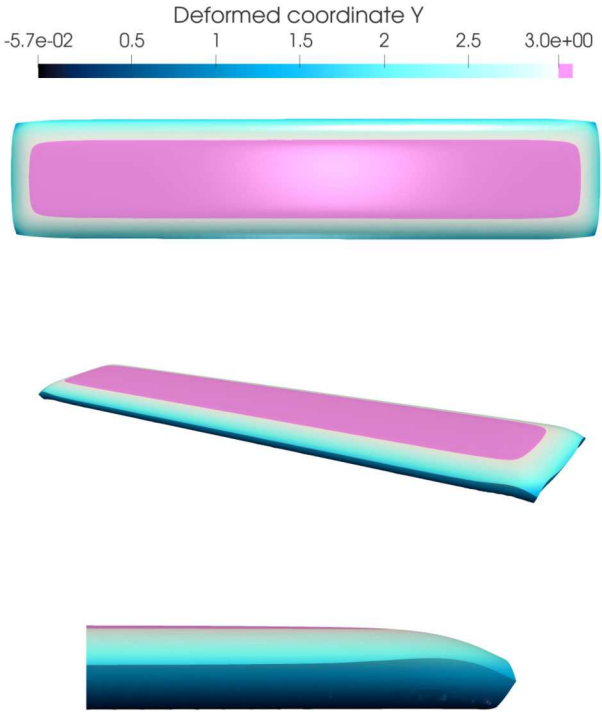

Fig. 5 Points $\mathbf{y} = (y_1, y_2, y_3) \in \boldsymbol{\varphi}(\Omega)$ colored in pink are those for which $y_2 \geq (0.95) \max_{\Omega} y_2$. The values of c and e in the last two rows of Table 1 correspond to the length and width of the essentially flat region formed by those magenta points

Both in experiments and in simulations (carried out with the above values of χ), most of the top surface remains essentially flat after the deformation, giving way to a rounding of the corners starting at a small distance from the edges. However, the definition of parameters c and e in Fig. 4 is subjective. In Table 1, the (arbitrarily chosen) criterion to measure parameters c and e from the affine model and the phantom model simulations was: $y_2 \geq (0.95)\max y_2$ (see Fig. 5).

4.2 Comparison of the Models – Lateral Swelling

The main parameters in the description of the lateral swelling are the total deformed length d and the total deformed width f. The relative errors in d for the affine and the phantom models, compared to experimental results, are, respectively, of -0.003% and of $+0.27\%$. The relative errors in f are, respectively, -0.8% and of $+0.9\%$. Therefore, in measurements d and f both models very precisely capture the lateral swelling of close to 2 mm on each side and there is no significative difference between the models.

Regarding parameter c, the relative errors for the affine and the phantom models are -0.7% and -1.5%. The relative errors for parameter e are of 8.7% and 5.7%. As explained before, the precise definition of this parameter is subjective and it is difficult to have a precise comparison between simulations and experiments.

The height b after deformation of the middle point of the edge at the top and at the right of the sample is the measurement in which the models depart most from the experiment. For the affine model the relative error is of -16.6% and for the phantom model it is of -18.5%. As for the height g of the middle point of the top edge of the front facet, the relative errors are -1.16% and -4.07%, respectively.

4.3 Comparison of the Models – Vertical Swelling

Due to the constraint imposed by the bonding surface, most of the deformation occurs in the direction normal to it. For example, the deformed width of 18.95 mm is 26.3% more than the reference width of 15 mm (and it is not observed for points of all heights, only those on the top surface), whereas the thickness increases by 110% (and the same holds for the height of most points in the sample). The relative errors in the affine and phantom models for the measurement a of this vertical swelling are, respectively, of -11.2% and -6.2%. Given the much more significant role of the extension in this direction as compared to the lateral extension in these experiments, and given the ability of both models to capture well the lateral swelling (with errors of less than 1% in the measurements d and f of the length and width after deformation), we conclude that this difference between a -11.2% and a -6.2% error in the estimation of the vertical extension is very significative, and that the agreement of the phantom model to the experiment is much better.

Apart from comparing the finite element simulations of both models against the experiments, we can also compared the experimentally observed vertical stretch against the theoretical prediction in the idealized thin-film limit [30] (Sect. 3.6), [4] (Sect. 3). This corresponds to a homogeneous uniaxial extension in which the normal component of the osmotic pressure on the top surface balances out with the normal component of the elastic forces, namely,

$$\mathbf{P}\Big(\mathrm{diag}(1,\lambda,1)\Big)\mathbf{n}=\mathbf{0},\quad \mathbf{n}=\mathbf{e}_2, \tag{49}$$

with the Piola-Kirchhoff tensor P being as in (45). For the affine and the phantom model this gives

$$\gamma\lambda_{\mathrm{uni}}-\frac{\gamma}{\lambda_{\mathrm{uni}}}+\ln(1-\frac{\phi_0}{\lambda_{\mathrm{uni}}})+\chi_{\mathrm{aff}}\frac{\phi_0^2}{\lambda_{\mathrm{uni}}^2}+\frac{\phi_0}{\lambda_{\mathrm{uni}}}=0 \quad\Rightarrow\quad \lambda_{\mathrm{uni}}\approx 1.88, \tag{50}$$

$$\gamma\lambda_{\mathrm{uni}}+\ln(1-\frac{\phi_0}{\lambda_{\mathrm{uni}}})+\chi_{\mathrm{ph}}\frac{\phi_0^2}{\lambda_{\mathrm{uni}}^2}+\frac{\phi_0}{\lambda_{\mathrm{uni}}}=0 \quad\Rightarrow\quad \lambda_{\mathrm{uni}}\approx 1.99. \tag{51}$$

The relative errors of these theoretical predictions against the measured vertical stretch of $\lambda = 2.10$ of Eq. (44) are, respectively, of -10.5% and -5.2%. This is consistent with the difference of the relative errors of -11.2% and -6.2% in the numerical simulations (where the aspect ratio $1.62/90 = 1.8\%$ is small but not zero).

We end this subsection by noting that the reduced swelling in the affine model compared to the prediction in the phantom model is observed not only in the vertical extension, corresponding to measurement a in Fig. 4, but in all of the parameters from a to g (that is, also in the measurements of the lateral swelling). Indeed, the main parameters d and f (deformed length and width) are smaller in the affine model. Regarding the heights b and g after the lateral facets of the gel roll over due to the lateral swelling, a larger value of these parameters in the affine model indicate that the top edge has not fallen down as much as it has done in the phantom model, which shows a less pronounced lateral swelling. Analogously, a larger value of c and e corresponds to a larger portion of the top surface that remains flat and a smaller effect of rounding of the top edges and corners, which is again indicative of a less pronounced lateral swelling.

4.4 Lateral Swelling in y_1 vs. Lateral Swelling in y_3

Both models capture the experimental observation of a lateral swelling that is more pronounced on the long edge of the gel (towards the back and the front) than on the short edges (towards the left and the right). The difference between d and c is $93.73 - 88.26 = 5.47$ mm whereas between f and e is $18.95 - 11.61 = 7.34$ mm. If these values are compared to the respective dimensions of 90 mm and 15 mm, the difference is more evident, as can be seen in the figure Fig. 5c) of the top view of the deformed gel in the simulation. Also, g is less than b in the experiments (they differ by 18.5%) and in the simulations with both models (differing by 4.1% in the model without the logarithmic term and by 3.4% in the model with the logarithmic term).

4.5 Rigorous Proof of the Reduced Vertical Swelling in the Affine Model

When fitting the model against the free swelling experiment, the logarithmic term favors expansions of the polymer network, hence a larger χ of 0.426 is obtained compared to the 0.348 in the model without $-G \ln J$. However, for the bonded experiment, the hydrophobic effect of the larger χ is more pronounced than the expansion favored by the $-G \ln J$ term. In the end, in this experiment the gel swells more in the model without the logarithmic term: 3.19 mm thickness compared to 3.02 mm; 93.98 mm length compared to 93.70 mm; 19.12 mm width compared to 18.80 mm.

To better understand this, which is not intuitive, let us state more precisely that we are comparing the $\lambda_{\text{uni}} \approx 1.99$ obtained using the model without the logarithmic term, with $\chi = 0.348$, against the $\hat{\lambda}_{\text{uni}} \approx 1.88$ obtained from the model with the logarithmic term, with $\hat{\chi} = 0.426$. The first comes from the equation

$$\gamma \lambda_{\text{uni}} + \ln(1 - \frac{\phi_0}{\lambda_{\text{uni}}}) + \chi \frac{\phi_0^2}{\lambda_{\text{uni}}^2} + \frac{\phi_0}{\lambda_{\text{uni}}} = 0 \tag{52}$$

while the second comes from

$$\gamma \hat{\lambda}_{\text{uni}} - \frac{\gamma}{\hat{\lambda}_{\text{uni}}} + \ln(1 - \frac{\phi_0}{\hat{\lambda}_{\text{uni}}}) + \hat{\chi} \frac{\phi_0^2}{\hat{\lambda}_{\text{uni}}^2} + \frac{\phi_0}{\hat{\lambda}_{\text{uni}}} = 0, \tag{53}$$

The values of χ and $\hat{\chi}$ come from the equations

$$\frac{\gamma}{\lambda_{\rm iso}} + \ln(1-\phi_{\rm iso}) + \chi\phi_{\rm iso}^2 + \phi_{\rm iso} = 0, \tag{54}$$

$$\frac{\gamma}{\lambda_{\rm iso}} - \frac{\gamma}{J_{\rm iso}} + \ln(1-\phi_{\rm iso}) + \hat{\chi}\phi_{\rm iso}^2 + \phi_{\rm iso} = 0. \tag{55}$$

The equations for $\lambda_{\rm uni}$, $\hat{\lambda}_{\rm uni}$, χ, and $\hat{\chi}$ are of the form

$$f(\chi(s), s) = 0, \quad g(\chi(s), \lambda(s), s) = 0, \tag{56}$$

with

$$f(\chi, s) = \frac{\gamma}{\lambda_{\rm iso}} - \frac{s}{J_{\rm iso}} + \ln(1-\phi_{\rm iso}) + \chi\phi_{\rm iso}^2 + \phi_{\rm iso}, \tag{57}$$

$$g(\chi, \lambda, s) = \gamma\lambda - \frac{s}{\lambda} + \frac{\partial H}{\partial J}(\chi, \lambda), \tag{58}$$

$$H(\chi, J) = (J-\phi_0)\ln(1-\frac{\phi_0}{J}) + \chi\phi_0(1-\frac{\phi_0}{J}), \tag{59}$$

taking $s = 0$ for $\lambda_{\rm uni}$, $s = \gamma$ for $\hat{\lambda}_{\rm uni}$ and $\chi(s), \lambda(s)$ being the functions of s defined implicitly by (56).

The dependence of f on both χ and s is affine, hence it can be seen easily that

$$\frac{\partial\chi}{\partial s} = -\frac{\partial f/\partial s}{\partial f/\partial\chi} = \frac{1/J_{\rm iso}}{\phi_{\rm iso}^2} = \frac{J_{\rm iso}}{\phi_0^2}. \tag{60}$$

Differentiating now $g\big(\chi(s), \lambda(s), s\big) = 0$ with respect to s we find that

$$\frac{\partial g}{\partial\lambda}\frac{\partial\lambda}{\partial s} = -\frac{\partial g}{\partial s} - \frac{\partial g}{\partial\chi}\frac{\partial\chi}{\partial s}, \tag{61}$$

$$\left(\gamma + \frac{s}{\lambda^2} + \frac{\partial^2 H}{\partial J^2}\right)\frac{\partial\lambda}{\partial s} = \frac{1}{\lambda(s)} - \frac{\phi_0^2}{\lambda(s)^2}\frac{J_{\rm iso}}{\phi_0^2} = -\frac{J_{\rm iso}-\lambda(s)}{\lambda(s)^2}. \tag{62}$$

The prefactor on the left-hand side of (62) is positive since H is convex in J for every fixed χ. On the other hand, as the strength s of the logarithmic term $-s\ln J$ added to the stored-energy density $\frac{\gamma}{2}|\mathbf{F}|^2 + H(J)$ increases from $s = 0$ to $s = \gamma$, the optimal uniaxial extension $\lambda(s) = \lambda_{\rm uni}(s)$ remains always below $J_{\rm iso}$ since $\lambda(s)$ is the Jacobian of the deformation gradient $\mathrm{diag}(1, \lambda(s), 1)$ for the uniaxial extension, and a confined gel never increases its volume more than in the free swelling experiment. All in all, $\lambda(s)$ is decreasing in s, that is, the bonded gel in the model with the logarithmic term swells less than in the model without it.

5 Conclusions

In this article, we set the stage for a thorough investigation of singular phenomena in gels, that further connects the mathematical aspects of the work with the triggering mechanisms, whether in the form of heat or ionic interaction. In particular, the former may be related with the *coffee ring* phenomenon that occurs by solvent evaporation, as explained by Doi [7]. In

future work, we aim at providing a measure theoretical study of the conservation of mass, involving the notion of *distributional determinant*, which will also allow us to extend our studies of singularities to dynamics.

Author contributions M.C. Calderer worked on the model, analysis and wrote part of the main manuscript text. D. Henao worked on the model, analysis and wrote part of the main manuscript text. M.A. Sanchez did the numerical simulations. R.A. Siegel contributed to the gel modeling, supervised the energetics component of the manuscript as well as the laboratory experiments. S. Song carried out all the laboratory experiments.

Funding S.S. and M.C.C. were funded by National Science Foundation grant DMS-1616866. M.S. was supported by FONDECYT Regular grant N. 1221189 and by Centro Nacional de Inteligencia Artificial CENIA, FB210017, Basal ANID Chile. D.H. was funded by FONDECYT 1190018.

Declarations

Competing interests The authors declare no competing interests.

References

1. Ball, J.M.: Convexity conditions and existence theorems in nonlinear elasticity. Arch. Ration. Mech. Anal. **63**, 337–403 (1977)
2. Ball, J.M.: Discontinuous equilibrium solutions and cavitation in nonlinear elasticity. Philos. Trans. R. Soc. Lond. Ser. A, Math. Phys. Sci. **306**, 557–611 (1982)
3. Bowen, R.M.: The thermochemistry of a reacting mixture of elastic materials with diffusion. Arch. Ration. Mech. Anal. **34**, 97–127 (1969)
4. Calderer, M.C., Garavito, C., Henao, D., Lyu, S., Tapia, L.: Gel debonding from a rigid substrate. J. Elast. **141**, 51–73 (2020)
5. Calderer, M.C., Zhang, H.: Incipient dynamics of swelling of gels. SIAM J. Appl. Math. **68**, 1641–1664 (2008)
6. Dacorogna, B.: Direct Methods in the Calculus of Variations. Springer, Berlin (1989)
7. Doi, M.: Soft Matter Physics. Oxford University Press, London (2013)
8. Dunwoody, N.: A thermomechanical theory of diffusion in solid-fluid mixtures. Arch. Ration. Mech. Anal. **38**, 348–371 (1970)
9. Dunwoody, N.: Balance laws for liquid crystal mixtures. Z. Angew. Math. Phys. **26**, 105–111 (1975)
10. Dunwoody, N., Müller, I.: A thermodynamic theory of two chemically reacting ideal gases with different temperatures. Arch. Ration. Mech. Anal. **29**, 344–369 (1968)
11. English, A., Mafé, S., Manzanares, J.A., Yu, X., Grosberg, A., Tanaka, T.: Equilibrium swelling properties of polyampholytic hydrogels. J. Chem. Phys. **104**, 8713–8720 (1996)
12. Ericksen, J.L.: Introduction to the thermodynamics of solids. Applied Mathematics, 2nd edn. Springer, New York (1997)
13. Flory, P.: Principles of Polymer Chemistry. Cornell University Press, Ithaca (1953)
14. Flory, P.J.: Thermodynamics of dilute solutions of high polymers. J. Chem. Phys. **13**, 453–465 (1945)
15. Flory, P.J., Rehner, J. Jr.: Statistical mechanics of cross-linked polymer networks I. Rubberlike elasticity. J. Chem. Phys. **11**, 512–520 (1943)
16. Flory, P.J., Rehner, J. Jr.: Effect of deformation on the swelling capacity of rubber. J. Chem. Phys. **12**, 412–414 (1944)
17. Song Gibbs, J.W.: On the equilibrium of heterogeneous substances. Am. J. Sci. **3**, 441–458 (1878)
18. Horkay, F.: Polyelectrolyte gels: a unique class of soft materials. Gels. Marine Gels **7**, 102–119 (2021)
19. Huggins, M.L.: Molecular weights of high polymers. Ind. Eng. Chem. **35**, 980–986 (1943)
20. Kang, M.K., Huang, R.: Swell-induced surface instability of confined hydrogel layers on substrates. J. Mech. Phys. Solids **58**, 1582–1598 (2010)
21. Knowles, J.: Large amplitude oscillations of a tube of incompressible elastic material. Quart. Appl. Math. **18**, 71–77 (1960)
22. Kundu, S., Crosby, A.J.: Cavitation and fracture behavior of polyacrylamide hydrogels. Soft Matter **5**, 3963–3968 (2009)
23. Mark, J.E., Erman, B.: Rubberlike Elasticity: A Molecular Primer, 2nd edn. Cambridge University Press, Cambridge (2007)

24. Müller, S., Qi, T., Yan, B.S.: On a new class of elastic deformations not allowing for cavitation. Ann. Inst. Henri Poincaré, Anal. Non Linéaire **11**, 217–243 (1994)
25. Pence, T.J., Tsai, H.: Swelling-induced cavitation of elastic spheres. Math. Mech. Solids **11**, 527–551 (2006)
26. Penrose, O., Lebowitz, J.L.: Towards a rigorous molecular theory of metastability. Fluct. Phenom. **7**, 293–340 (1987)
27. Ricka, J., Tanaka, T.: Swelling of ionic gels: quantitative performance of the Donnan theory. Macromolecules **17**, 2916–2921 (1984)
28. Rubinstein, M., Colby, R.H., et al.: Polymer Physics, vol. 23. Oxford University press, New York (2003)
29. Schöberl, J.: C ++ 11 implementation of finite elements in NGSolve. In: Tech. Rep., vol. 30. Vienna University of Technology – Institute for Analysis and Scientific Computing, Vienna (2014)
30. Song, S., Siegel, R.A., Sánchez, M.A., Calderer, M.C., Henao, D.: Experiments, modelling, and simulations for a gel bonded to a rigid substrate. J. Elast. (2022). https://doi.org/10.1007/s10659-022-09911-6
31. Tanaka, T.: Collapse of gels and the critical endpoint. Phys. Rev. Lett. **12**, 820–823 (1978)
32. Tanaka, T., Filmore, D.: Kinetics of selling of gels. J. Chem. Phys. **70**, 1214–1218 (1979)
33. Tanaka, T., Sato, E.: Patterns in shrinking gels. Nature **358**, 482–485 (1992)
34. Weiner, J.: Statistical Mechanics of Elasticity, 2nd edn. Dover, New York (2017)
35. Hong, J.W., Zhao, X., Suo, Z.: A theory of coupled diffusion and large deformation in polymeric gels. J. Mech. Phys. Solids **56**, 1779–1793 (2008)
36. Zhang, H.: Static and dynamical problems of hydrogel swelling: Modeling and analysis. PhD thesis, University of Minnesota (2007)

Authors and Affiliations

M. Carme Calderer[1] · Duvan Henao[2] · Manuel A. Sánchez[3] · Ronald A. Siegel[4] · Sichen Song[4,1]

✉ M.C. Calderer
calde014@umn.edu

D. Henao
duvan.henao@uoh.cl

M.A. Sánchez
manuel.sanchez@ing.puc.cl

R.A. Siegel
siege017@umn.edu

S. Song
song0357@umn.edu

1 School of Mathematics, University of Minnesota, Minneapolis, MN 55455, USA

2 Instituto de Ciencias de la Ingeniería, Universidad de O'Higgins, Rancagua, Chile

3 Instituto de Ingeniería Matemática y Computacional, Pontificia Universidad Católica de Chile, Santiago, Chile

4 Department of Pharmaceutics, University of Minnesota, Minneapolis, MN 55455, USA